

Atmospheric Fe supply and marine productivity in the Glacial North Pacific

Ocean

François Burgay^{1,2}, Andrea Spolaor^{1*}, Jacopo Gabrieli¹, Giulio Cozzi¹, Clara Turetta¹, Paul Vallelonga^{3,4}, Carlo Barbante^{1,2}

¹Institute of Polar Sciences, National Research Council. Via Torino, 155, 3100 Venice (Italy)

²Department of Environmental Sciences, Informatics and Statistics, Ca' Foscari University of Venice. Via Torino, 155 – Venice (Italy)

³Physics of Ice Climate and Earth, Niels Bohr Institute, University of Copenhagen. Tagensvej 16, Copenhagen N2200 (Denmark)

⁴Oceans Graduate School, University of Western Australia (Australia)

* Corresponding author: andrea.spolaor@unive.it

Abstract

Iron is a key element in the Earth climate system as it can enhance the marine primary productivity in the high-nutrient low-chlorophyll (HNLC) regions where, despite a high concentration of major nutrients, the chlorophyll production is low due to iron limitation. Aeolian mineral dust represents one of the main Fe sources to the oceans; thus, quantifying its variability over the last glacial cycle is crucial to evaluate its role in strengthening the biological carbon pump. Polar ice cores, which preserve detailed climate records in their stratigraphy, provide a sensitive and continuous archive for reconstructing past aeolian Fe fluxes. Here, we show the Northern Hemisphere Fe record retrieved from the NEEM ice core (Greenland), which offers a unique opportunity to reconstruct the past Fe fluxes in a portion of the Arctic over the last 108 kyr. Holocene Fe fluxes (0.042 -11.7 kyr b2k, 0.5 mg m⁻² yr⁻¹) at the NEEM site were four times lower than the average recorded over the last glacial period (11.7– 108 kyr b2k, 2.0 mg m⁻² yr⁻¹), while they were greater during the Last Glacial Maximum (LGM, 14.5 – 26.5 kyr b2k, 3.6 mg m⁻² yr⁻¹) and Marine Isotope Stage 4 (MIS 4, 60 - 71 kyr b2k, 5.8 mg m⁻² yr⁻¹). Comparing the NEEM Fe record with palaeoceanographic records retrieved from the HNLC

26 North Pacific, we found that the coldest periods, characterized by the highest Fe fluxes, were characterized by
27 a low marine primary productivity in the subarctic Pacific Ocean, likely due to the greater sea-ice extent and
28 the absence of major nutrients upwelling. This supports the hypothesis that Fe-fertilization during colder and
29 dustier periods (i.e. LGM and MIS 4) was more effective in other regions, such as the mid-latitude North
30 Pacific, where a closer relationship between marine productivity and the NEEM Fe fluxes was observed.

31 **1. Introduction**

32 Greenland and Antarctic ice cores are unique archives that can provide records of temperature, atmospheric
33 dust load and atmospheric gas composition variability during the Holocene and the late Pleistocene (Jouzel et
34 al., 1996; Lambert et al., 2008; Schüpbach et al., 2018; Watanabe et al., 2003). Glacial periods were dustier
35 and characterized by a lower CO₂ concentration (≈ 180 ppm) than interglacials (≈ 280 ppm) (Lambert et al.,
36 2008; Lüthi et al., 2008). This dichotomy is explained through several different hypotheses: the increase in
37 aridity and newly exposed continental shelves (Fuhrer et al., 1999), an increase in the aerosol atmospheric life-
38 time resulted from a reduced hydrological cycle (Lambert et al., 2008; Yung et al., 1996), increased glacial-
39 derived mobilization of highly bioavailable iron (Fe) from physical breakdown of bedrock (Shoenfelt et al.,
40 2018), and, lastly, more vigorous polar circulation capable of entraining additional dust from lower latitudes
41 (Mayewski et al., 1994). Regardless of the source, the higher atmospheric burden of mineral dust during glacial
42 periods affected climate through both physical and biological mechanisms. Dust particles can directly
43 influence the Earth's radiative budget by scattering, absorbing and re-emitting shortwave and longwave
44 radiation (Miller and Tegen, 1998; Schepanski, 2018). During the LGM, model results showed that the
45 enhanced dust transport caused, alone, a 1.0 W/m² globally averaged radiative forcing decrease compared to
46 present day conditions, which contributed to a 0.85°C cooling relative to the current climate (Mahowald et al.,
47 2006). Conversely, once deposited on the ocean surface, the mineral dust delivered major and micronutrients
48 (including Fe) that could have stimulated the biological carbon pump (Martin et al., 1990). Indeed, Fe can limit
49 marine primary production (MPP) in the high-nutrient low-chlorophyll (HNLC) oceans, which are
50 characterized by a high concentration of nutrients, but low productivity (Martin et al., 1990). The largest ones
51 are the Southern Ocean, the Equatorial Pacific and the North Pacific Ocean (Duggen et al., 2010). In these
52 regions, the Fe role in modulating marine productivity was demonstrated through both artificial Fe fertilization
53 experiments (Smetacek et al., 2012; Tsuda et al., 2003; Yoon et al., 2018) and natural Fe inputs from iceberg

54 melting, volcanic eruptions and glacially sourced dust (Duprat et al., 2016; Langmann et al., 2010; Shoenfelt
55 et al., 2017). For its biological relevance, it has been hypothesized that the recorded decrease in the atmospheric
56 CO₂ concentration during glacial periods was linked to the Fe-modulated enhancement of the biological carbon
57 pump in the HNLC regions due to the increase in Fe availability (Martin et al., 1990). Evidences for the
58 existence of a strong link between atmospheric Fe deposition and marine productivity were retrieved from a
59 marine sediment core collected in the subantarctic zone of the Southern Ocean where, the coldest periods were
60 mirrored by an increase in atmospheric Fe fluxes and by an enhancement of both MPP and degree of nutrient
61 consumption (Martínez-García et al., 2014). Yet, according to both modeling (Lambert et al., 2015) and
62 observational (Gaspari et al., 2006; Röthlisberger, 2004; Vallelonga et al., 2013) studies, the Fe-fertilization
63 mechanism itself cannot completely explain the ≈ 100 ppmv glacial-interglacial atmospheric CO₂ variability,
64 but only around 8-20 ppmv of it (Lambert et al., 2015).

65 However, the role of Fe fertilization in the Northern Hemisphere and in the HNLC region of the North
66 Pacific is unclear due to the few available Arctic Fe flux records which are either limited to the last century or
67 they only cover short time periods (Burgay et al., 2019; Hiscock et al., 2013). Thus, reconstructing how the Fe
68 concentrations and fluxes have changed in the Northern Hemisphere during the last glacial cycle is essential
69 to understand the evolution of the global atmospheric circulation, the human impact on dust mobilization
70 (Mahowald et al., 2008) and to evaluate, as well, the impact that Fe might have had on MPP in the North
71 Pacific HNLC region. Here, we present a high-resolution 108 kyr record of total dissolvable Fe (TDFe)
72 retrieved from the North Greenland Eemian Ice Drilling (NEEM) ice core (Rasmussen et al., 2013; Schüpbach
73 et al., 2018), which provides a unique insight on the atmospheric Fe supply in the Arctic both during the
74 Holocene and the last glacial period. Furthermore, we performed a comparison between the TDFe NEEM
75 record and various palaeoproductivity records from the HNLC North Pacific region (Figure 1) to evaluate
76 whether the increase in aeolian Fe fluxes was mirrored by an increase in marine productivity. We underline
77 that, TDFe concentrations, as it will be discussed in the following, derives from the acidification of the snow
78 samples for 1 month at pH 1. Thus, they represent an upper limit of the aeolian Fe potentially available for the
79 phytoplankton, and it might overestimate the actual bioavailable Fe.

80 **2. Materials and methods**

81 **2.1 Sampling and processing**

82 In the framework of the NEEM project, a 2540 m-depth ice core was drilled in north-western
83 Greenland (77°45'N, 51°06'W) at 2479 m.a.s.l. The site is characterized by an average annual temperature of
84 -29°C and a modern accumulation of 22 cm ice equivalent per year. According to the GICC05modelext-
85 NEEM-1 timescale, the ice core covers the last 128 kyrs (Rasmussen et al., 2013). The ice cores were cut to
86 obtain ice sticks with a square cross section of 36x36 mm. They were continuously melted on a continuous
87 flow analysis (CFA) system with a typical melt-speed of 3.5 cm min⁻¹ (Schüpbach et al., 2018). The CFA
88 system provides meltwater from the inner and least likely to be contaminated part of the core, thus we did not
89 adopt any further decontamination procedure. The ICP-MS samples were manually collected at a low-
90 resolution (110 cm). The temporal resolution depends on the accumulation rate and it decreases with depth
91 because of the ice thinning. According to the available timescale (Rasmussen et al., 2013) and considering the
92 110 cm sampling resolution, the temporal resolution varies from decadal to millennial (Table 1).

93 Samples were collected in vials previously cleaned as follows: 7 days with HNO₃ 5% (Suprapure,
94 Romil, UK), rinsed three times with ultrapure water (UPW, Elga, UK), 7 days with HNO₃ 2% (Suprapure,
95 Romil, UK), rinsed three times with UPW and then stored in HNO₃ 1% (Ultrapure, Romil, UK) until the day
96 before the sample collection, when they were rinsed three times with UPW and dried overnight under a laminar
97 flow hood Class 100. The samples were kept frozen and shipped to Italy for analysis. Once melted, the samples
98 were acidified to pH 1 using HNO₃ (Suprapure, Romil, UK). To ensure an effective dissolution of Fe particles,
99 samples were stored at room temperature and analysed 30 days after the acidification without any additional
100 filtration step. We adopted this approach since the analysis immediately after the acidification step might have
101 led to uncertainties attributable to the Fe dissolution kinetics (Edwards, 1999; Koffman et al., 2014). Our
102 choice was consistent with other studies that indicate that samples to be used for calculation of atmospheric
103 fluxes must be acidified for at least 1 month prior to analysis to avoid any possible misinterpretation of the
104 trace-element data (Koffman et al., 2014). We will refer to this fraction as total dissolvable Fe (TDFe) which
105 includes both the most labile fraction (dissolved iron, DFe), which is rendered soluble under mildly acidic
106 conditions (Hiscock et al., 2013), and the fraction enclosed in iron-bearing mineral particles. TDFe does not
107 directly represent the actual bioavailable Fe that can be dissolved into seawater at pH 8, but, considering that

108 TDFe and DFe are significantly correlated (Du et al., 2020; Xiao et al., 2020), an upper limit of the aeolian
109 Fe potentially available for the phytoplankton (Edwards et al., 2006).

110 **2.2 Analytical procedure and performances**

111 The ice samples were analysed with an Inductively Coupled Plasma Single Quadrupole Mass Spectrometer
112 (ICP-qMS, Agilent 7500 series, USA) equipped with a quartz Scott spray chamber for the determination of
113 Ca, Na and Fe. To minimize any kind of contamination, all the instrument tubes were flushed before the
114 analysis for 2 hours with 2% HNO₃ (Suprapure, Romil, UK). A 120 seconds rinsing step with 2% HNO₃
115 (Suprapure, Romil, UK) occurred after each sample analysis to reduce any possible memory effect. The vials
116 used for the standard preparation were cleaned following the same procedure adopted for the ice samples.
117 Considering the isobaric and polyatomic interferences affecting Fe, this element was quantified using the
118 interference-free isotope ⁵⁷Fe. External calibration curves with acidified standards (2% HNO₃, Suprapure,
119 Romil, UK) were prepared for Ca, Na and Fe from dilution of a certified single-element 1000 ppm ± 1%
120 standard solution (Fisher Chemical, USA). The resulting R² for the external calibration curves was 0.999 for
121 all the elements. The Limit of Detection (LoD) for ⁵⁷Fe, calculated as three times the standard deviation of the
122 blank, was 0.8 µg L⁻¹. To assess accuracy for Fe, the TM-RAIN04 certified reference material (National
123 Research Council of Canada) was measured every 50 samples. The accuracy was determined as a recovery
124 percentage calculated as O/T %, where O is the determined value and T is the certified value. For Fe, the
125 accuracy was 104%, while precision, calculated as Relative Standard Deviation (RSD %) of selected samples
126 read multiple times (n = 5) during the analysis, was on average 5% (7% for samples (n = 3) from the interglacial
127 period, 4% for samples (n = 3) from the last glacial period). For Ca and Na, the LoD was 1 µg L⁻¹ and 3 µg L⁻¹,
128 respectively. In the absence of a certified reference material, Ca and Na accuracy was calculated using a
129 Quality Control (QC) sample prepared at 10 µg L⁻¹ and measured every 50 samples. Accuracy for Ca and Na,
130 calculated as described above, was 94% and 108%, respectively, while precision (RSD%) was on average 6%
131 (4% for samples from the interglacial period and 7% for samples from the last glacial period) and 2% (for both
132 periods), respectively.

133 Non-sea-salt Ca concentration is commonly used as proxy for terrestrial inputs in polar regions and it is
134 calculated as $nssCa = [Ca] - ([Ca]/[Na])_{sw} \cdot [Na]$, where sw indicates seawater.

135 3. Results and discussion

136 3.1 Fe fluxes from the NEEM core

137 Fe and nssCa concentrations and fluxes were calculated as $F = C \cdot A$ (where F is the Fe flux, in mg m^{-2}
138 yr^{-1} , C is the Fe or nssCa concentration, in ng g^{-1} , and A the accumulation, in m yr^{-1} ice equivalent, previously
139 determined by Rasmussen et al., 2013). A pattern of higher dust (expressed as nssCa^{2+}) and Fe fluxes during
140 colder climate periods and lower dust and Fe fluxes during warmer climate periods is clearly recognizable
141 (Figure 2).

142 The Holocene (0.042 -11.7 kyr b2k) was characterized by average Fe fluxes of $0.5 \text{ mg m}^{-2} \text{ yr}^{-1}$ that
143 varied between $0.01 \text{ mg m}^{-2} \text{ yr}^{-1}$ and $5.3 \text{ mg m}^{-2} \text{ yr}^{-1}$ (Figure 2). The coefficient of variability (CV), calculated
144 as the ratio between the standard deviation and the mean value, was 1.2. The more recent 4000 years are
145 characterized by the highest average Fe fluxes ($0.6 \pm 0.4 \text{ mg m}^{-2} \text{ yr}^{-1}$). The lowest Fe fluxes were recorded
146 between 4000 and 8000 years b2k ($0.3 \pm 0.2 \text{ mg m}^{-2} \text{ yr}^{-1}$). During the Younger Dryas (YD, 11.7 – 12.9 kyr
147 b2k), an abrupt cooling was observed with a drop in the $\delta^{18}\text{O}$ value from -36.9‰ to -43.1‰ . Coincidentally, the
148 recorded average Fe fluxes rose to $1.2 \pm 0.4 \text{ mg m}^{-2} \text{ yr}^{-1}$, higher than both the 12.9-13.9 kyr b2k ($0.5 \pm 0.3 \text{ mg}$
149 $\text{m}^{-2} \text{ yr}^{-1}$) and the 10.7- 11.7 kyr b2k ($0.3 \pm 0.2 \text{ mg m}^{-2} \text{ yr}^{-1}$) periods.

150 The last glacial period (11.7-108 kyr b2k) showed Fe fluxes four-times higher ($2.0 \pm 2.2 \text{ mg m}^{-2} \text{ yr}^{-1}$)
151 than the Holocene, spanning from 0.05 to $16.5 \text{ mg m}^{-2} \text{ yr}^{-1}$ (Figure 2). However, a significant variability during
152 the last glacial period was detected. During the LGM and MIS 4, average Fe fluxes were 7 ($3.6 \pm 2.3 \text{ mg m}^{-2}$
153 yr^{-1}) and 10-times ($5.8 \pm 2.8 \text{ mg m}^{-2} \text{ yr}^{-1}$) greater than the Holocene average. Fe fluxes also increased during
154 the MIS 5c-MIS5b transition (87 kyr b2k), when a concurrent decrease in $\delta^{18}\text{O}$ values was observed. During
155 MIS 5c and MIS 5d, Fe fluxes were comparable with those detected during the Holocene. The high frequency
156 of the Dansgaard-Oeschger (D-O) events during MIS 3, was mirrored by the high variability in both nssCa and
157 Fe fluxes. Each stadial period corresponded to an increase in both Fe and nssCa. However, their variability
158 was significantly different. During MIS 3, Fe fluxes showed maximum values greater than $5 \text{ mg m}^{-2} \text{ yr}^{-1}$ during
159 D-O 4, 9, 12, 15 ($8.5, 6.5, 7.5, 6.6 \text{ mg m}^{-2} \text{ yr}^{-1}$ respectively), and lower than $5 \text{ mg m}^{-2} \text{ yr}^{-1}$ during D-O 6, 7, 8,
160 10, 11 and 13 ($3.9, 2.6, 4.1, 2.6, 2.7, 3.2 \text{ mg m}^{-2} \text{ yr}^{-1}$ respectively). This variability was significantly higher
161 than the one recorded for nssCa, which showed maximum values close to $20 \text{ mg m}^{-2} \text{ yr}^{-1}$ for all the D-O events.

162 **3.2 Comparison with Fe fluxes from Antarctic ice cores**

163 The NEEM Fe ice core record allows the first comparison of Fe concentrations and fluxes between the
164 Arctic and Antarctica (Figure 3, Table 3). The only Antarctic Fe records that can reach at least the LGM are
165 from Talos Dome (TD) (Spolaor et al., 2013; Vallelonga et al., 2013), Law Dome (LD) (Edwards et al., 2006;
166 Edwards et al., 1998) and EPICA Dome C (EDC) (Wolff et al., 2006). However, we point out that both the
167 samples from Dome C and Talos Dome were acidified for at least 24 hours, leading to a possible
168 underestimation of the actual TDFe concentration. This implies that the general trends and features can be
169 comparable with the NEEM record, while absolute concentrations might differ due to the different acidification
170 procedure used (Koffman et al., 2014).

171 During the Holocene, in Antarctica, the average Fe flux and concentration values varied significantly
172 among the different sites with similar values recorded at the coastal sites (TD) and lower values in the internal
173 Antarctic Plateau (EDC) (Table 3). For TD, this was explained both through changes in atmospheric transport
174 patterns across Antarctica and through an additional local input of dust from proximal Antarctic ice-free zones
175 that affected coastal sites more than the central plateau, which was exclusively exposed to remote sources such
176 as southern South America (Albani et al., 2012; Delmonte et al., 2010b; Vallelonga et al., 2013).

177 During the LGM, both TD and EDC shared a similar dust flux loading, comprised between 10 and 15 mg
178 $\text{m}^{-2} \text{yr}^{-1}$ (Baccolo et al., 2018), and the same dust source region, as confirmed by the Sr-Nd isotopes (Delmonte
179 et al., 2010a). Compared to the Holocene, in TD the atmospheric dust fluxes increased of a factor 6, while in
180 EDC the increase was approximately of a factor 25 (Delmonte et al., 2010b). This is mirrored by a similar
181 average Fe fluxes enhancement compared to the Holocene with values that were up to 4 and 21-fold higher,
182 respectively (Vallelonga et al., 2013; Wolff et al., 2006). The reason of these discrepancies between the two
183 sites is likely due to the higher Holocene dust flux observed in TD compared to EDC, as a consequence of a
184 relevant local dust contribution at TD (Baccolo et al., 2018; Delmonte et al., 2010b).

185 During the last glacial period, the most relevant dust source was southern South America for both TD and
186 EDC (Basile et al., 1997; Delmonte et al., 2010b; Lambert et al., 2008). Dust fluxes peaked during MIS 4
187 where both sites recorded maximum values around $10 \text{ mg m}^{-2} \text{yr}^{-1}$ (Lambert et al., 2008; Vallelonga et al.,

188 2013) and comparable Fe fluxes ($0.17 \pm 0.07 \text{ mg m}^{-2} \text{ yr}^{-1}$ at TD and $0.12 \pm 0.07 \text{ mg m}^{-2} \text{ yr}^{-1}$ at EDC) (Vallelonga
189 et al., 2013; Wolff et al., 2006).

190 The LD record, due to the different analytical preparation of the samples, is not directly comparable with
191 TD and EDC. Nevertheless, we can still evaluate and discuss the Fe flux ratio between the Holocene and the
192 LGM. Unfortunately, for the LD record, there is no dust profile available, meaning that it is not possible to
193 assess which is the main dust and Fe sources for this location, although the Australian continent has been an
194 important source of mineral dust in the recent past (Edwards et al., 2006; Vallelonga et al., 2002). During the
195 LGM, Fe fluxes increased 10-fold compared to the Holocene period, 2.5 times more than what was observed
196 in TD. Similarly to what observed in the EDC record, this difference might be explained either by the absence
197 of local dust sources that affected LD during the Holocene, or by the lower sampling frequency for the LD
198 record ($n = 27$) compared to TD ($n = 801$).

199 Despite the different acidification times, the overall picture during the Holocene is that the average Fe
200 fluxes in NEEM ($0.5 \text{ mg m}^{-2} \text{ yr}^{-1}$, $CV = 1.2$) were higher than in Antarctica. Among the Antarctic Fe fluxes,
201 TD ($0.09 \text{ mg m}^{-2} \text{ yr}^{-1}$, $CV = 1.2$) and LD ($0.04 \text{ mg m}^{-2} \text{ yr}^{-1}$, $CV = 0.5$) were higher than the ones recorded at
202 EDC ($0.007 \text{ mg m}^{-2} \text{ yr}^{-1}$, $CV = 0.2$).

203 In NEEM, the LGM (19 – 26.5 kyr b2k) was characterized by a 10-fold and 7-fold enhancement in dust
204 (expressed as nssCa) and Fe fluxes, respectively. A similar behaviour was observed in the Antarctic cores as
205 described above (Table 3). Considering that the atmospheric CO_2 concentration dropped down to 180 ppm
206 (Köhler et al., 2017), the global Fe fluxes enhancement likely contributed to part of this decrease, promoting
207 marine productivity in some HNLC regions (Amo and Minagawa, 2003; Kawahata et al., 2000; Martínez-
208 Garcia et al., 2011).

209 During MIS 4 (60-71 kyr b2k), NEEM Fe fluxes were higher compared to all the other investigated
210 records. Compared to the LGM average, during MIS 4, dust (Ruth, 2007), nssCa and Fe fluxes (this work) in
211 the Arctic exhibited a ≈ 1.5 -fold increase (Table 3), while they were lower both in TD and EDC. To explain
212 this behaviour we advance some hypotheses. The first is that the increase in dust and Fe fluxes can be
213 attributable to changes in the atmospheric circulation, likely due to the topographic influence of the Laurentide
214 Ice Sheet (LIS). Indeed, during the LGM, LIS was nearly 2 times larger than at MIS 4 (Löfverström et al.,

215 2014; Tulenko et al., 2020) and it might have caused a stronger meridional splitting of the westerlies
216 (Löfverström et al., 2014) and a southward migration of their mean position (Kang et al., 2015; Manabe and
217 Broccoli, 1985). The southward shift during the LGM might have produced a reduction of strong winds passing
218 over the source areas (i.e. Taklimakan and Gobi deserts) (Kang et al., 2015) and/or a stronger southward Fe
219 and dust deposition over the Chinese Loess Plateau (Zhang et al., 2014) and the mid-latitude North Pacific
220 (Sun et al., 2018). In contrast, during MIS 4, the westerlies might have been located northward (i.e. over the
221 Taklimakan and Gobi deserts) and characterized by a less marked meridional splitting (Löfverström et al.,
222 2014), conveying a larger amount of dust to Greenland. We also propose two alternative hypotheses that rely
223 on 1) the possibility that additional dust sources (e.g. Saharan dust) might have reached Greenland during MIS
224 4, and 2) that during MIS 4, the Asian monsoon system was stronger in winter than in summer, producing drier
225 conditions that caused an enhanced dust production and transport to Greenland (Xiao et al., 1999). However,
226 to better address this point, a more comprehensive investigation that involves a large set of palaeorecords and
227 atmospheric modelling is required and it is beyond the scope of the manuscript.

228 **3.3 Comparison with lower-resolution Fe NEEM measurements**

229 A parallel study that reported Fe concentration from the NEEM ice core was recently published (Xiao et
230 al., 2020). It reports the TDFe and DFe concentration and fluxes with a lower temporal resolution ($n = 166$)
231 than the current investigation ($n = 1596$). Moreover, the analytical approach was different since the melted ice
232 samples were filtered at $0.45 \mu\text{m}$ and acidified for six weeks before the analysis. Even though the overall
233 pattern between the two records is similar, we observe several differences between Xiao et al., (2020) and our
234 study: a) the average Fe concentration over the entire record is 4-fold higher than the one found in our
235 investigation (101.4 ng g^{-1} vs 20.4 ng g^{-1}); b) the Fe concentration range is wider ($1.5\text{-}1194.5 \text{ ng g}^{-1}$ vs $>\text{LoD} -$
236 457.6 ng g^{-1}) compared to the data presented in this manuscript; c) average Fe fluxes are 2.4-fold higher during
237 the Holocene ($1.2 \text{ mg m}^{-2} \text{ yr}^{-1}$ vs $0.5 \text{ mg m}^{-2} \text{ yr}^{-1}$) and 3.5-fold higher during the LGM ($12.5 \text{ mg m}^{-2} \text{ yr}^{-1}$ vs 3.6
238 $\text{mg m}^{-2} \text{ yr}^{-1}$) that the ones recorded in this study; d) the LGM Fe flux showed a 10-fold increase during the
239 Holocene, compared to the 7-fold enhancement that we observed; e) TDFe fluxes and concentration are higher
240 during the LGM than during MIS 4, while we found higher fluxes during MIS 4, consistently with a similar
241 enhancement of nssCa and dust (Ruth, 2007).

242 Possible reasons of these differences might rely on the different temporal resolution and on the
243 discrepancies between the adopted analytical approaches that highlight the need to standardize the analytical
244 procedures when trace elements are analyzed in ice and snow samples in order to have a more reliable
245 comparison among both different and identical locations.

246 **3.4 Fe and marine productivity in the Northern Hemisphere**

247 Considering the biological relevance of Fe and taking advantage from the Fe flux record retrieved from
248 the NEEM ice core, one important question remains regarding whether its flux increase during the last glacial
249 period triggered the marine productivity in the HNLC region of the North Pacific (Olgun et al., 2011).

250 Nowadays, a significant amount of Asian dust (250 Mt yr^{-1}) is primarily deposited over the HNLC region
251 of the subarctic Pacific (Serno et al., 2014; Zhang et al., 2003) and the marine productivity changes in this
252 oceanic region might reflect potential Fe fertilization effects promoted by atmospheric Fe supply. During
253 modern times, both increases in aeolian influx from Asia (Young et al., 1991) and sporadic Fe input from
254 volcanic eruptions (Langmann et al., 2010) resulted in enhanced MPP by more than 60%. Moreover, recent
255 Fe-fertilization experiments performed south of the Gulf of Alaska (McDonald et al., 1999; Tsuda et al., 2003),
256 showed significant increases in the abundance of diatoms and in chlorophyll-a concentration (Boyd et al.,
257 1996), indicating that the North Pacific is maybe sensitive to atmospheric Fe inputs. However, no data are
258 available to evaluate if the Fe-sensitivity of the subarctic Pacific Ocean holds even over longer timescales and,
259 if an increase in the aeolian Fe supply, observed during glacial periods, could explain the MPP variability in
260 the subarctic Pacific Ocean. To address this point, we compared the NEEM Fe record with different marine
261 sediment cores (Table 4).

262 Previous geochemical evidence indicates that for both interglacial and glacial periods the dust source
263 influencing Greenland and the North Pacific mainly originated from the East Asian deserts (Schüpbach et al.,
264 2018; Serno et al., 2014). However, considering that there are no aeolian Fe flux records from the marine
265 sediment cores, they might have received different amount of Fe compared to what observed in the ice core
266 record. Through a comparison between a marine sediment record from the western subarctic Pacific Ocean
267 (SO202-07-6) and the NGRIP ice core, it has been shown that dust fluxes changed coherently and
268 simultaneously during abrupt climate changes, even though with different amplitude (Serno et al., 2015). The

269 larger variability observed in NGRIP, as well as in NEEM, than in marine sediments, indicates changes in the
270 atmospheric dust transport from the source areas to Greenland (e.g. rate of aerosol rainout, different wind
271 strength).

272 Recently, it has been proposed that additional dust sources might have influenced Greenland in the last
273 31 kyrs (Han et al., 2018; Lupker et al., 2010). Strontium and lead isotopes indicate that Saharan dust
274 contributed to the overall NEEM dust budget during the Younger Dryas (12-73%) and between 17 kyrs and
275 22 kyrs (16-70%), while the Taklimakan and Gobi contribution (i.e. eastern Asia sources) was dominant (55-
276 94%) prior to 22 kyrs (Han et al., 2018). However, despite the Saharan dust source, we assume that the main
277 dust source for the NEEM ice core during the last glacial period is represented by the Gobi and Taklimakan
278 deserts (Svensson et al., 2000). This is coherent with the dust changes synchronicity among Greenland, the
279 Chinese loess (Ruth et al., 2007) and the Northern Pacific sediment records located downwind of the Asian
280 dust sources (Schüpbach et al., 2018; Serno et al., 2015). Nevertheless, additional investigations to assess the
281 magnitude of the Saharan dust contribution prior to 31 kyrs and to identify other possible source regions are
282 needed.

283 All variables considered (i.e. different dust amplitude and other potential dust sources), and observing
284 that the overall pattern of higher dust deposition during the coldest periods is consistent between the ice and
285 sediment core records, we assumed that the Fe flux changes observed in NEEM are representative for the
286 aeolian Fe supply to the subarctic Pacific Ocean.

287 To evaluate whether past marine productivity was influenced by atmospheric Fe supply for the period
288 ranging from the LGM to the Holocene, we compared the NEEM record with the high temporal resolution
289 SO202-27-6 (from the Patton-Murray Rise plateau, eastern subarctic Pacific Ocean) and the SO202-07-6 (from
290 the Detroit Seamount, western subarctic Pacific Ocean) productivity records (Méheust et al., 2018). For a long-
291 term record, we relied on the ODP887 (McDonald et al., 1999) and the ODP882 (Haug et al., 1995) sediment
292 cores, located close to SO202-27-6 and SO202-07-6, respectively. A comparison over the last 108 kyr between
293 the NEEM record and the S-2 sediment core (from the Shatsky Rise, mid-latitude North Pacific) was also
294 performed (Amo and Minagawa, 2003) (Figure 4, Table 4).

295 The past marine primary productivity reconstruction was performed relying on the Si/Al ratio, % of
296 biogenic silica and brassicasterol concentration. Si/Al ratio is used as a proxy for opal, or biogenic silica
297 (diatoms), in the absence of directly measured opal concentrations. The normalization to Al removes any
298 possible variable inputs of lithogenic detritus (McDonald et al., 1999). Brassicasterol is a sterol compound
299 which has been used as a molecular indicator of the presence of diatoms (Sachs and Anderson, 2005).
300 Brassicasterol concentration is also used, together with highly branched isoprenoid alkenes (IP₂₅), for the PIP₂₅
301 calculation, which is a proxy for the evaluation of past sea-ice conditions (Méheust et al., 2018; Müller et al.,
302 2011)

303 **3.4.1 From the LGM to the Holocene**

304 During the Last Glacial Maximum, the Fe fluxes recorded in the NEEM ice core were 7 times higher
305 compared to the Holocene. However, marine productivity in the subarctic Pacific Ocean, expressed as Si/Al
306 ratio (McDonald et al., 1999), % biogenic silica (Haug et al., 1995) and brassicasterol concentration (Méheust
307 et al., 2018), was at its lowest level (Figures 4, 5). Reconstructions based on the foraminifera-bound $\delta^{15}\text{N}$ (FB-
308 $\delta^{15}\text{N}$), a proxy which indicates the degree of nitrate consumption by phytoplankton (Martínez-García et al.,
309 2014), showed that, in the western subarctic Pacific Ocean, the nitrate consumption was more complete during
310 the LGM and the YD (i.e. when MPP was low) compared to the warmest periods (Ren et al., 2015). In other
311 words, during the coldest and dustiest periods, the nitrate consumption efficiency was higher (i.e. increase in
312 the FB- $\delta^{15}\text{N}$ values) than during the interglacials, even though MPP was low. This apparent contradiction can
313 be explained by an increase in water stratification (either by reduced upwelling or vertical mixing), where the
314 most nutrient-rich and oxygen depleted waters were shifted to deeper depths, while nutrient-depleted and
315 better-ventilated waters rested above a hydrographic boundary at 1500-2000 m (Kohfeld and Chase, 2017).
316 Water stratification led to minimal input of nutrients to the surface ocean, leading the system towards a major
317 nutrient limitation (Kienast et al., 2004; Ren et al., 2015). Among the several possible reasons that can explain
318 the increase in water stratification in the Glacial North Pacific, we propose two hypotheses. The first relies on
319 the glacial closure of the Bering Strait that reduced the freshwater export from the Pacific Ocean to the Atlantic,
320 retaining more freshwater in the North Pacific (Talley, 2008). The second involves sea-ice formation. When
321 sea-ice forms, in the Okhotsk and Bering Seas, brine rejection occurs, increasing water density and creating
322 the more saline and denser North Pacific Intermediate Water (NPIW). When the wind blows the sea-ice away

323 from where it was originally formed, brine rejection can further proceed at the same location following the
324 formation of new sea-ice. The continuous brine rejection promotes the freshening of surface waters and
325 strengthens water stratification (Costa et al., 2018).

326 An additional explanation for the observed lower productivity during glacial periods arises from the
327 higher extent of perennial sea-ice that might have played a role in creating a physical barrier between the
328 atmosphere and the marine environment, reducing the amount of available sunlight and the direct deposition
329 of bioavailable Fe on the seawater surface (Kienast et al., 2004; Méheust et al., 2018). Marine sediment records,
330 collected in the eastern and western subarctic Pacific and in the Bering Sea, showed extended spring ice-cover
331 during the LGM (Méheust et al., 2018; Méheust et al., 2016) when the Fe fluxes were at their maxima. The
332 progressive decrease in perennial sea-ice coverage recorded after the LGM led to an increase in the marine
333 productivity (Figure 5), with a maximum during the Bølling-Allerød (B/A) warm event (\approx 13-15 kyr ago). The
334 possible relevance of sea-ice in modulating MPP at the highest latitude of the Pacific Ocean during the LGM
335 is strengthened by a marine sediment record collected in the mid-latitude North Pacific (Amo and Minagawa,
336 2003), which, because of its southernmost location, did not experience any sea-ice condition. During the LGM,
337 contrarily to what is observed in the subarctic Pacific, a prominent maximum in marine productivity was
338 recorded, suggesting that Fe could have triggered an important phytoplankton response (Figure 4d). The Fe-
339 sensitivity of the mid-latitude North Pacific is confirmed during the Holocene, when the Fe fluxes were at their
340 minima and the productivity, expressed as MAR (mass accumulation rate) C_{37} alkenone ($\mu\text{g cm}^{-2} \text{ kyr}^{-1}$), was
341 at its lowest level. A plausible explanation is that stratified waters did not characterize this region during the
342 last glacial period and thus it was not affected by the limitation of major nutrients. Unfortunately, neither FB-
343 $\delta^{15}\text{N}$ nor information about water stratification are available for this record.

344 However, there might be other reasons that could explain the strengthening in MPP during the B/A
345 warm period in the subarctic North Pacific. Among them, we propose the increase in the sea-level that
346 inundated previously exposed lands which might have entrained iron and other nutrients to the marine
347 ecosystem (Davies et al., 2011), or changes in the oceanic circulation (McManus et al., 2004). Indeed, at the
348 onset of the B/A event, the meridional overturning circulation rapidly accelerated and this might have produced
349 an upward displacement of the nutrient-rich North Pacific Deep Water towards intermediate depths, promoting
350 an injection of nutrients to surface waters and enhancing marine productivity.

351 These additional explanations shed light on the marginal role that atmospheric Fe fertilization had in
352 promoting MPP in the subarctic Pacific Ocean since other players might have had a more significant impact
353 (Kohfeld and Chase, 2017).

354 **3.4.2 From 108 kyr to the LGM**

355 According to the available records, marine productivity changed heterogeneously in the Pacific Ocean
356 during the last glacial period (Figure 4).

357 It is challenging to state, with a high degree of confidence, whether Fe-fertilization triggered a
358 phytoplankton bloom or not in the HNLC subarctic North Pacific. This is due to the different responses that
359 the western and the eastern side of the subarctic North Pacific showed with respect to the atmospheric Fe
360 supply (Figure 4). In the eastern subarctic Pacific, the increase in the aeolian Fe fluxes was mirrored by a
361 phytoplankton response during the MIS 5.2 and the MIS 5 / MIS 4 transition. The subsequent decrease in MPP
362 during the MIS 4 suggests that the prolonged Fe supply during the coldest stadial might have led the ecosystem
363 towards the limitation of other nutrients (Kienast et al., 2014) following the same mechanisms described in the
364 previous section. The enhanced water stratification during those periods, as suggested by stable oxygen isotope
365 ratios in planktonic foraminifera (Zahn et al., 1991), did not allow a supply of macronutrients from below the
366 mixed layer. Thus, additional atmospheric Fe supply had little effect on phytoplankton productivity, suggesting
367 their growth was likely limited by the lack of major nutrients (Kienast et al., 2004). In the western subarctic
368 Pacific, the increase in productivity was recorded also in periods with low atmospheric Fe fluxes (e.g. from
369 100 to 90 kyr at ODP882), strengthening the hypothesis that other influences (e.g. meltwater inputs, continental
370 margin supply, sea-ice) had a more relevant role (Kienast et al., 2004; Lam and Bishop, 2008) than atmospheric
371 Fe supply.

372 On the contrary to what was observed in the subarctic Pacific, the S-2 sediment core collected in the
373 mid-latitude North Pacific (Amo and Minagawa, 2003), showed a marked increase in marine primary
374 productivity during MIS 4 and the overall last glacial period when the Fe fluxes were higher (Figure 4). MPP
375 in the mid-latitude North Pacific might have been more sensitive to the atmospheric Fe supply, suggesting that
376 the high degree of upper ocean stratification that characterized the subarctic region of the Pacific Ocean did
377 not affect the mid-latitude North Pacific allowing for a continuous supply of macronutrients. The observed

378 increase in dust transport (and Fe deposition) could have then stimulated marine productivity (Kienast et al.,
379 2004).

380 **4. Conclusions and future perspectives**

381 In this study, we provided a high-temporal-resolution Fe record from mineral dust input retrieved from the
382 NEEM ice core. Through the comparison with other available Fe records, we observed that Fe fluxes were
383 higher in Greenland than in Antarctica. The greatest difference between Arctic and Antarctic records occurred
384 during MIS4, when Fe fluxes in NEEM were 1.5 times higher than during the LGM, while, in TD and EDC,
385 they were lower. To explain this behaviour, we advanced two hypotheses (i.e. change in the atmospheric
386 circulation or additional dust sources that reached Greenland), even though more detailed investigations are
387 needed.

388 Merging our record with marine productivity data, we found that a link between Fe transport and ocean
389 productivity holds in the mid-latitude North Pacific, indicating that this area might be sensitive to the
390 atmospheric Fe supply. On the contrary, in the subarctic Pacific, we did not find any overwhelming evidence
391 that the increase in the atmospheric Fe fluxes triggered a phytoplankton response. This indicates that other
392 players, such as sea-ice and increased water stratification during the coldest periods had a more relevant role
393 in modulating the MPP in the HNLC region of the North Pacific on a millennial time scale.

394 This study provides an upper limit for estimating the potentially bioavailable Fe supplied to marine
395 phytoplankton in the North Pacific region, however additional studies should focus on analysing the labile and
396 bioavailable Fe fractions to constrain realistic Fe supply and response of the marine ecosystem.

397 **Data availability**

398 Data will be published on Pangaea

399 **Author contributions**

400 FB wrote the manuscript. FB, AS and CB designed the research. JG, CT and GC performed the analyses. PV
401 contributed to the interpretation of the results.

402 **Competing interests**

403 The authors declare that they have no conflict of interest.

404 **Acknowledgments**

405 We sincerely thank all the persons involved in the logistics, drilling operations, ice-core processing and sample
406 collection. NEEM is directed and organized by the Center of Ice and Climate at the Niels Bohr Institute and
407 US NSF Office of Polar Programs and it is supported by funding agencies and institutions in Belgium (FNRS-
408 CFB and FWO), Canada (NRCan/GSC), China (CAS), Denmark (FIST), France (IPEV, CNRS/INSU, CEA
409 and ANR), Germany (AWI), Iceland (RannIs), Japan (NIPR), Korea (KOPRI), The Netherlands (NWO/ALW),
410 Sweden (VR), Switzerland (SNF), United Kingdom (NERC), and the USA (US NSF, Office of Polar
411 Programs).

412 We are grateful to the three anonymous reviewers and to the editor that contributed to the overall improvement
413 of the manuscript.

414

415 **Figures and tables**

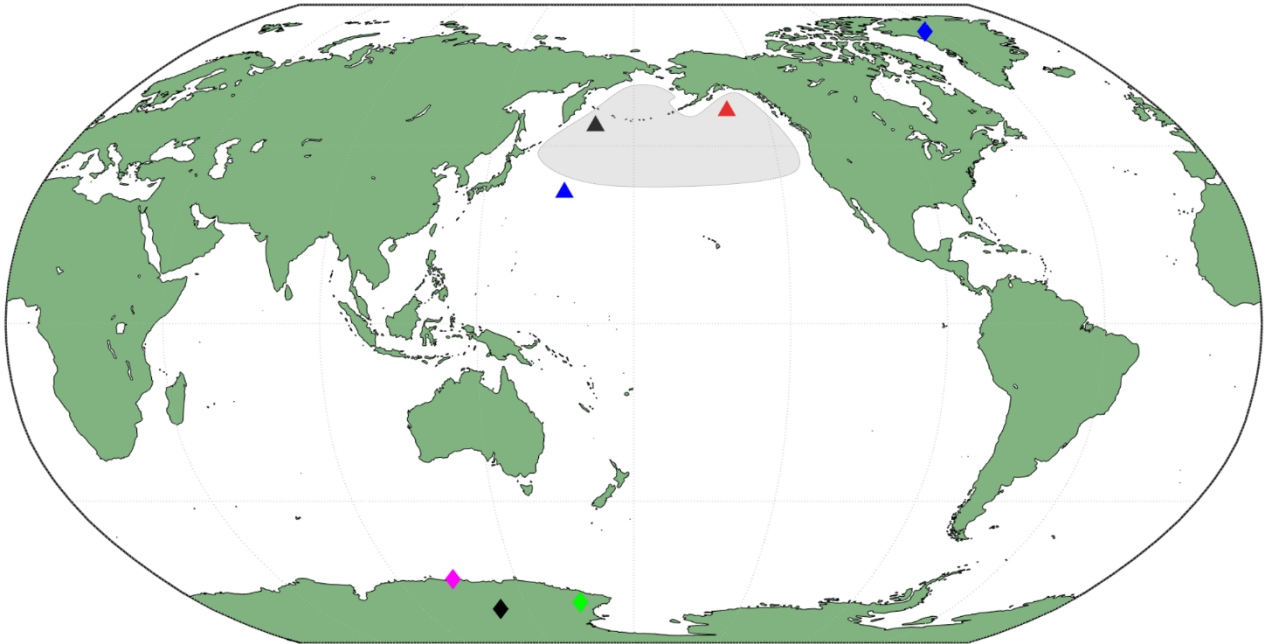
416

417 **Figure 1** - Locations of the NEEM ice core (blue diamond, this study), the LD ice core (pink triangle, Edwards
418 et al., 2006), EDC ice core (black diamond, Wolff et al., 2006) and TD ice core (green diamond, Vallelonga
419 et al., 2013). We retrieved palaeoproductivity data for the eastern North Pacific (black triangle) from the
420 ODP882 (Haug et al., 1995) and SO202-27-6 (Méheust et al., 2018) sediments cores, while for the western
421 Pacific Ocean (red triangle) from the ODP887 (McDonald et al., 1999) and SO202-07-6 (Méheust et al., 2018)
422 sediment cores. The palaeoproductivity record from the mid-latitude North Pacific was retrieved from the S-2
423 sediment core (blue triangle, Amo and Minagawa, 2003).

424

425

426



427

428

429

430

431

432

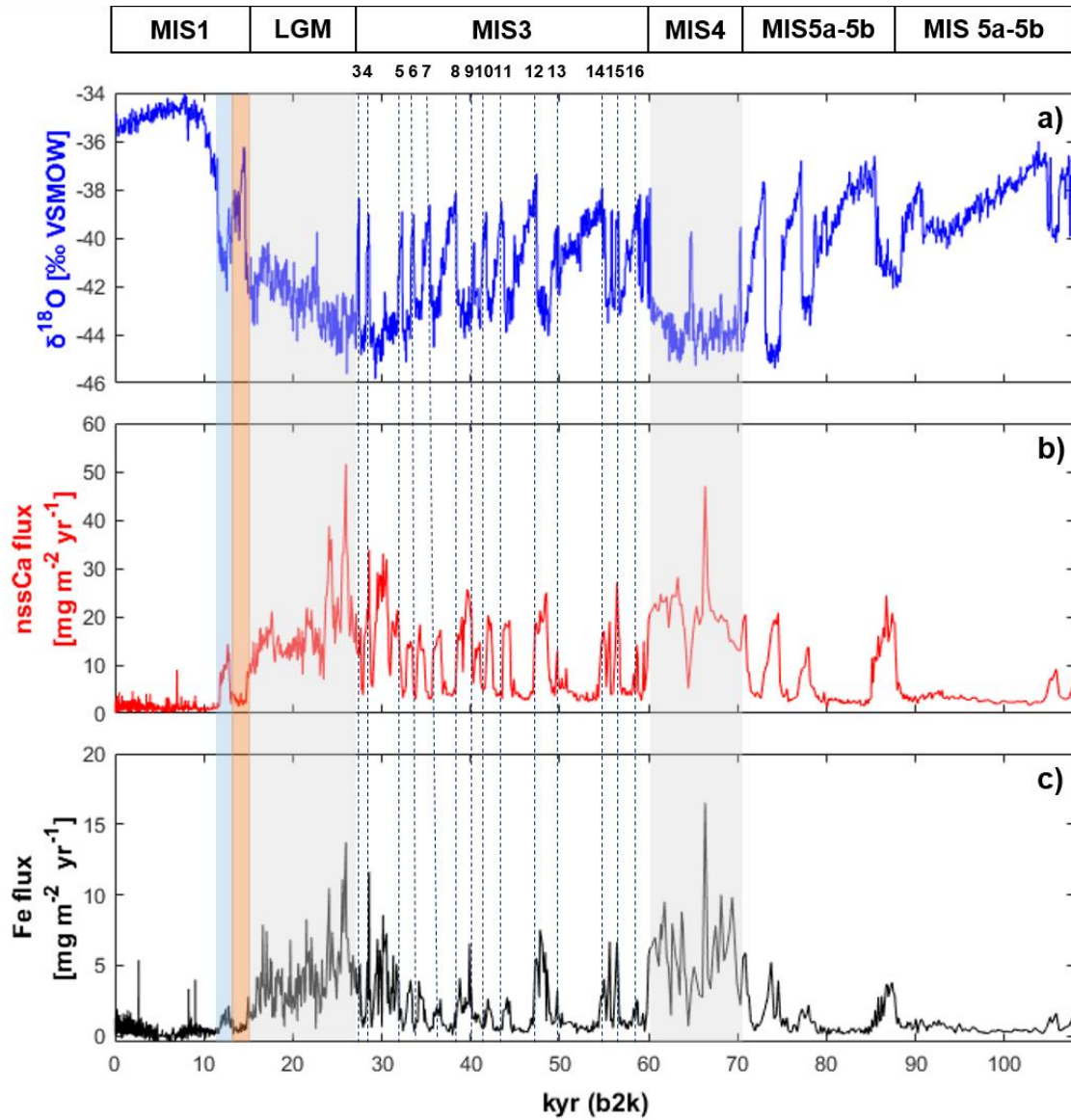
433

434

435

436 **Figure 2** – Panel a) $\delta^{18}\text{O}$ (blue line) profile is from the NGRIP ice core (North Greenland Ice Core Project,
437 2007). Panel b) *nss*Ca flux (red line) from the NEEM ice core. Panel c) and Fe flux (black line) from the NEEM
438 ice core. Shaded blue rectangle: Younger Dryas. Shaded orange rectangle: Bølling-Allerød. Numbers in the
439 upper panel indicate the Dansgaard-Oeschger events from 3 to 16.

440



441

442

443

444

445

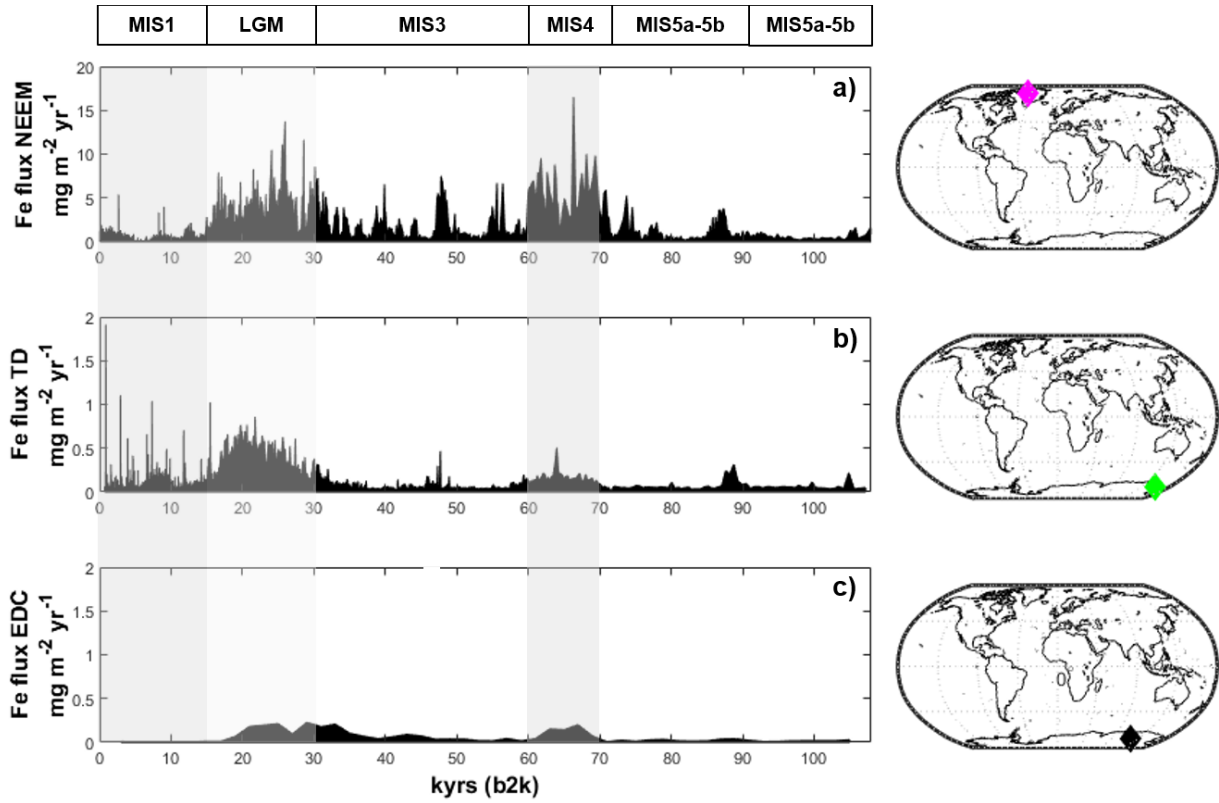
446

447

448 **Figure 3** – Comparison of the Fe fluxes among a) NEEM (this work, pink diamond), b) TD (Vallelonga et al.,
449 2013; green diamond) and c) EDC (Wolff et al., 2006; black diamond). Note that the y-axis for NEEM ranges
450 from 0 to 20 $\text{mg m}^{-2} \text{yr}^{-1}$, while the y-axis for TD and EDC ranges from 0 to 2 $\text{mg m}^{-2} \text{yr}^{-1}$.

451

452



453

454

455

456

457

458

459

460

461

462

463

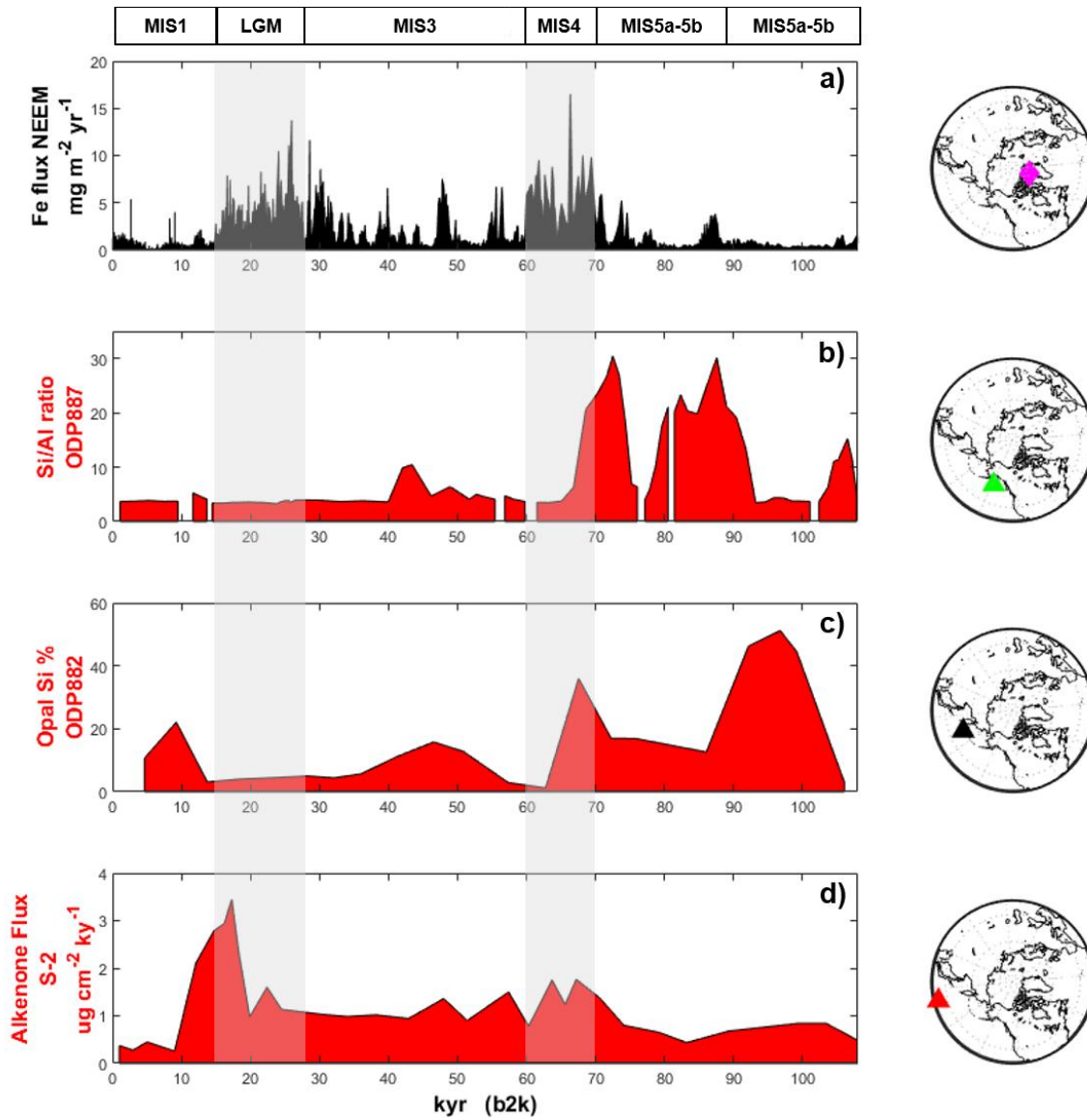
464

465

466

467 **Figure 4** – Comparison between Fe fluxes (black line, panel a) from NEEM (this work; pink diamond), with
 468 marine productivity (red line, panel b) from ODP887, eastern subarctic Pacific (McDonald et al., 1999; green
 469 triangle), ODP882 (red line, panel c), western subarctic Pacific (Haug et al., 1995; black triangle) and S-2 (red
 470 line, panel d), mid-latitude North Pacific (Amo and Minagawa, 2003; red triangle). Due to their limited
 471 temporal extension, productivity records from SO202-07-6 and SO202-07-26 are not discussed in this figure,
 472 but in Figure 4.

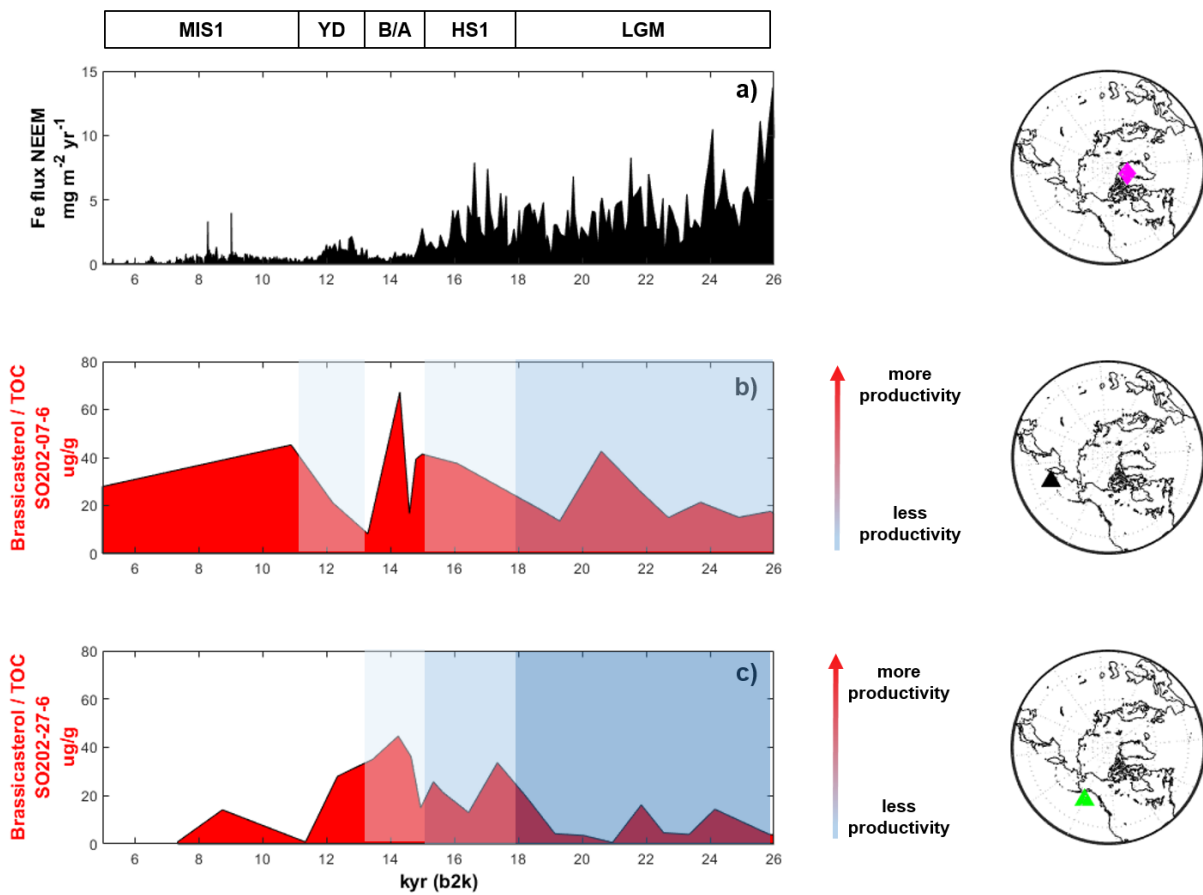
473



474

475 **Figure 5** – Relationship between Fe flux in the NEEM core, and MPP in subarctic Pacific Ocean over the last
 476 26 kyr, where higher brassicasterol-total organic carbon ratio represents an increase in productivity. Sea-ice
 477 data are from Meheust et al. (2018): prevalently extended sea-ice (dark blue rectangle), prevalently marginal
 478 sea-ice (blue rectangle), prevalently variable sea-ice (light blue rectangle), prevalently ice-free (white rectangle). Fe flux record (black line, panel a),
 479 productivity in the eastern subarctic Pacific Ocean (SO202-07-6, red line, panel b) and productivity in the western subarctic Pacific Ocean (SO202-27-6,
 480 red line, panel c) and productivity in the western subarctic Pacific Ocean (SO202-27-6, red line, panel c). Productivity pulses were recorded when sea-ice
 481 changed its conditions towards ice-free conditions. YD =
 482 Younger Dryas, B/A = Bolling-Allerod event, HS1 = Heinrich Stadial 1, LGM = Last Glacial Maximum.

483



484

485

486

487

488

489

490 **Table 1** - Temporal resolution of NEEM ice core, accordingly with the GICC05modelext-NEEM-1 age scale
 491 (Rasmussen et al., 2013). Ice samples for ICP-MS analysis were collected with a resolution of 110 cm.

492

Temporal resolution	Period
10 years	Holocene (present-7.2 kyr)
22 years	Holocene (7.2 kyr-LGM)
110 years	Last Glacial Maximum
73 years	Interstadials
147 years	28-59 kyr
440 years	59-70 kyr
220 years	70-96 kyr
730 years	96-110 kyr

493

494

495

496 **Table 2** – Fe and nssCa average concentration (ng g^{-1}) and fluxes ($\text{mg m}^{-2} \text{yr}^{-1}$) from the NEEM ice core. More
 497 details in the text. The coefficient of variability (CV) was calculated for Fe and nssCa fluxes and it is reported
 498 in bold.

	Fe average concentration /ng g^{-1}	Fe average fluxes $\text{/mg m}^{-2} \text{yr}^{-1}$	nssCa average concentration /ng g^{-1}	nssCa average fluxes $\text{/mg m}^{-2} \text{yr}^{-1}$
Holocene (0.042 -11.7 kyr b2k)	2.9	0.5 (CV 1.2)	7.2	1.4 (CV 2.3)
Glacial (11.7– 108 kyr b2k)	44.3	2.0 (CV 1.1)	210.8	10.0 (CV 0.8)
Younger Dryas (11.7 – 12.9 kyr b2k)	18.2	1.2 (CV 0.3)	135.2	8.5 (CV 0.4)
LGM (14.5 – 26.5 kyr b2k)	86.3	3.6 (CV 0.6)	273.3	12.3 (CV 0.7)
MIS 3 (26.5 – 60 kyr b2k)	45.5	1.9 (CV 1.0)	216.6	10.2 (CV 0.8)

MIS 4 (60 - 71 kyr b2k)	146.4	5.8 (CV 0.5)	510.2	20.5 (CV 0.3)
MIS 5a-MIS 5b (71-87 kyr b2k)	17.0	1.1 (CV 1.0)	98.6	6.3 (CV 0.8)
MIS 5c-MIS 5d (87-108 kyr b2k)	6.5	0.8 (CV 0.8)	50.4	4.3 (CV 0.9)

499

500

501

502

503

504 **Table 3** – Comparison of average Fe concentration ([Fe] in ng g^{-1}) and fluxes (in $\text{mg m}^{-2} \text{yr}^{-1}$) among four
505 different ice cores: NEEM, Talos Dome (Vallelonga et al., 2013), Law Dome (Edwards et al., 2006) and Dome
506 C (Wolff et al., 2006). n.a. = not available. Average Fe concentration at DC is not available since the
507 accumulation rate at that site during MIS4 is unavailable. Data from Law Dome spans from 59 to 8.5 b2k (for
508 the Holocene) and from 18.2 to 23.7 b2k (for the LGM). The coefficient of variability (CV) was calculated for
509 Fe fluxes and it is reported in bold for all the cores.

510

	Greenland		Antarctica					
	NEEM		Talos Dome		Law Dome		Dome C	
	[Fe] / ng g^{-1}	Fe flux / $\text{mg m}^{-2} \text{yr}^{-1}$	[Fe] / ng g^{-1}	Fe flux / $\text{mg m}^{-2} \text{yr}^{-1}$	[Fe] / ng g^{-1}	Fe flux / $\text{mg m}^{-2} \text{yr}^{-1}$	[Fe] / ng g^{-1}	Fe flux / $\text{mg m}^{-2} \text{yr}^{-1}$
Holocene (0.042 -11.7 kyr b2k)	2.9	0.5 (CV 1.2)	1.4	0.09 (CV 1.2)	0.09	0.04 (CV 0.5)	0.2	0.007 (CV 0.2)
LGM (14.5 -26.5 kyr b2k)	86.3	3.6 (CV 0.6)	10.3	0.4 (CV 0.5)	2.4	0.4 (CV 0.7)	16	0.15 (CV 0.5)
MIS4 (60- 71 kyr b2k)	146.4	5.8 (CV 0.5)	3.1	0.17 (CV 0.4)	n.a.	n.a.	n.a.	0.12 (CV 0.6)

LGM/Holocene ratio	30	7	7	4	27	10	80	21
MIS4/LGM ratio	1.7	1.5	0.3	0.4	n.a.	n.a.	n.a.	0.8

511

512

513 **Table 4** – Summary of locations and data source for all the cores (both ice and sediment cores) discussed in
514 the text (NH = Northern Hemisphere; SH = Southern Hemisphere)

Name	Core	Location	Reference	Latitude/Longitude
NEEM ice	Ice core	NH	<i>This work</i>	77°45'N, 51°06'W
Talos Dome	Ice core	SH	Vallelonga et al., 2013	73°0'S 158°0'E
Law Dome	Ice core	SH	Edwards et al., 2006	66°46'S 112°48'E
Dome C	Ice core	SH	Wolff et al., 2006	75°06'S; 123°23' E
ODP882	Marine sediment	NH	Haug et al., 1995	50°22'N; 167°36'E
ODP887	Marine sediment	NH	McDonald et al., 1999	54°22'N; 148°27'W
SO202-27-6	Marine sediment	NH	Meheust et al., 2018	54°12'N; 149°36'W
SO202-07-6	Marine sediment	NH	Meheust et al., 2018	51°16'N; 167°42'E
S-2	Marine sediment	NH	Amo and Minagawa, 2003	33°22'N; 159°08'E

515

516

517 **References**

- 518 Albani, S., Delmonte, B., Maggi, V., Baroni, C., Petit, J. R., Stenni, B., Mazzola, C., and Frezzotti, M.:
519 Interpreting last glacial to Holocene dust changes at Talos Dome (East Antarctica): implications for
520 atmospheric variations from regional to hemispheric scales, *Clim. Past*, 8, 741-750, 2012.
521
- 522 Amo, M. and Minagawa, M.: Sedimentary record of marine and terrigenous organic matter delivery to the
523 Shatsky Rise, western North Pacific, over the last 130 kyr, *Organic Geochemistry*, 34, 1299-1312, 2003.
524
- 525 Baccolo, G., Delmonte, B., Albani, S., Baroni, C., Cibirin, G., Frezzotti, M., Hampai, D., Marcelli, A., Revel, M.,
526 and Salvatore, M.: Regionalization of the atmospheric dust cycle on the periphery of the East Antarctic ice
527 sheet since the last glacial maximum, *Geochemistry, Geophysics, Geosystems*, 19, 3540-3554, 2018.
528
- 529 Basile, I., Grousset, F. E., Revel, M., Petit, J. R., Biscaye, P. E., and Barkov, N. I.: Patagonian origin of glacial
530 dust deposited in East Antarctica (Vostok and Dome C) during glacial stages 2, 4 and 6, *Earth and Planetary
531 Science Letters*, 146, 573-589, 1997.
532
- 533 Boyd, P., Muggli, D., Varela, D., Goldblatt, R., Chretien, R., Orians, K., and Harrison, P.: In vitro iron
534 enrichment experiments in the NE subarctic Pacific, *Marine Ecology Progress Series*, 136, 179-193, 1996.
535
- 536 Burgay, F., Erhardt, T., Lunga, D. D., Jensen, C. M., Spolaor, A., Vallelonga, P., Fischer, H., and Barbante, C.:
537 Fe²⁺ in ice cores as a new potential proxy to detect past volcanic eruptions, *Science of The Total
538 Environment*, 654, 1110-1117, 2019.
539
- 540 Costa, K. M., McManus, J. F., and Anderson, R. F.: Paleoproductivity and Stratification Across the Subarctic
541 Pacific Over Glacial-Interglacial Cycles, *Paleoceanography and Paleoclimatology*, 33, 914-933, 2018.
542
- 543 Davies, M., Mix, A., Stoner, J., Addison, J., Jaeger, J., Finney, B., and Wiest, J.: The deglacial transition on the
544 southeastern Alaska Margin: Meltwater input, sea level rise, marine productivity, and sedimentary anoxia,
545 *Paleoceanography*, 26, 2011.
546
- 547 Delmonte, B., Andersson, P., Schöberg, H., Hansson, M., Petit, J., Delmas, R., Gaiero, D. M., Maggi, V., and
548 Frezzotti, M.: Geographic provenance of aeolian dust in East Antarctica during Pleistocene glaciations:
549 preliminary results from Talos Dome and comparison with East Antarctic and new Andean ice core data,
550 *Quaternary Science Reviews*, 29, 256-264, 2010a.
551
- 552 Delmonte, B., Baroni, C., Andersson, P. S., Schoberg, H., Hansson, M., Aciego, S., Petit, J. -R., Albani, S.,
553 Mazzola, C., Maggi, V., and Frezzotti, M.: Aeolian dust in the Talos Dome ice core (East Antarctica,
554 Pacific/Ross Sea sector): Victoria Land versus remote sources over the last two climate cycles, *Journal of
555 Quaternary Science*, 25, 1327-1337, 2010b.
556
- 557 Du, Z., Xiao, C., Mayewski, P. A., Handley, M. J., Li, C., Ding, M., Liu, J., Yang, J., and Liu, K.: The iron records
558 and its sources during 1990–2017 from the Lambert Glacial Basin shallow ice core, East Antarctica,
559 *Chemosphere*, 251, 126399, 2020.
560
- 561 Duggen, S., Olgun, N., Croot, P., Hoffmann, L. J., Dietze, H., Delmelle, P., and Teschner, C.: The role of
562 airborne volcanic ash for the surface ocean biogeochemical iron-cycle: a review, *Biogeosciences (BG)*, 7,
563 827-844, 2010.
564
- 565 Duprat, L. P., Bigg, G. R., and Wilton, D. J.: Enhanced Southern Ocean marine productivity due to
566 fertilization by giant icebergs, *Nature Geoscience*, 9, 219, 2016.
567

568 Edwards, R., Sedwick, P., Morgan, V., and Boutron, C.: Iron in ice cores from Law Dome: A record of
569 atmospheric iron deposition for maritime East Antarctica during the Holocene and Last Glacial Maximum,
570 *Geochemistry, Geophysics, Geosystems*, 7, 12, 2006.
571

572 Edwards, R., Sedwick, P. N., Morgan, V., Boutron, C. F., and Hong, S.: Iron in ice cores from Law Dome, East
573 Antarctica: implications for past deposition of aerosol iron, *Annals of Glaciology*, 27, 365-370, 1998.
574 Edwards, R. P. R.: Iron in modern and ancient East Antarctic snow: Implications for phytoplankton
575 production in the Southern Ocean, 1999. University of Tasmania, 1999.
576

577 Fuhrer, K., Wolff, E. W., and Johnsen, S. J.: Timescales for dust variability in the Greenland Ice Core Project
578 (GRIP) ice core in the last 100,000 years, *Journal of Geophysical Research: Atmospheres*, 104, 31043-31052,
579 1999.
580

581 Gaspari, V., Barbante, C., Cozzi, G., Cescon, P., Boutron, C., Gabrielli, P., Capodaglio, G., Ferrari, C., Petit, J.,
582 and Delmonte, B.: Atmospheric iron fluxes over the last deglaciation: Climatic implications, *Geophysical
583 Research Letters*, 33, 3, 2006.
584

585 Han, C., Do Hur, S., Han, Y., Lee, K., Hong, S., Erhardt, T., Fischer, H., Svensson, A. M., Steffensen, J. P., and
586 Vallelonga, P.: High-resolution isotopic evidence for a potential Saharan provenance of Greenland glacial
587 dust, *Scientific reports*, 8, 1-9, 2018.
588

589 Haug, G., Maslin, M., Sarnthein, M., Stax, R., and Tiedemann, R.: 20. EVOLUTION OF NORTHWEST PACIFIC
590 SEDIMENTATION PATTERNS SINCE 6 MA (SITE 882), 1995, 293.
591

592 Hiscock, W. T., Fischer, H., Bigler, M., Gfeller, G., Leuenberger, D., and Mini, O.: Continuous flow analysis of
593 labile iron in ice-cores, *Environmental science & technology*, 47, 4416-4425, 2013.
594

595 Jouzel, J., Waelbroeck, C., Malaize, B., Bender, M., Petit, J., Stievenard, M., Barkov, N., Barnola, J., King, T.,
596 and Kotlyakov, V.: Climatic interpretation of the recently extended Vostok ice records, *Climate Dynamics*,
597 12, 513-521, 1996.
598

599 Kang, S., Roberts, H. M., Wang, X., An, Z., and Wang, M.: Mass accumulation rate changes in Chinese loess
600 during MIS 2, and asynchrony with records from Greenland ice cores and North Pacific Ocean sediments
601 during the Last Glacial Maximum, *Aeolian Research*, 19, 251-258, 2015.
602

603 Kawahata, H., Okamoto, T., Matsumoto, E., and Ujiie, H.: Fluctuations of eolian flux and ocean productivity
604 in the mid-latitude North Pacific during the last 200 kyr, *Quaternary Science Reviews*, 19, 1279-1291, 2000.
605

606 Kienast, S. S., Hendy, I. L., Crusius, J., Pedersen, T. F., and Calvert, S. E.: Export production in the subarctic
607 North Pacific over the last 800 kyrs: No evidence for iron fertilization?, *Journal of Oceanography*, 60, 189-
608 203, 2004.
609

610 Koffman, B. G., Handley, M. J., Osterberg, E. C., Wells, M. L., and Kreutz, K. J.: Dependence of ice-core
611 relative trace-element concentration on acidification, *Journal of Glaciology*, 60, 103-112, 2014.
612

613 Kohfeld, K. E. and Chase, Z.: Temporal evolution of mechanisms controlling ocean carbon uptake during the
614 last glacial cycle, *Earth and Planetary Science Letters*, 472, 206-215, 2017.
615

616 Köhler, P., Nehrbass-Ahles, C., Schmitt, J., Stocker, T. F., and Fischer, H.: Continuous record of the
617 atmospheric greenhouse gas carbon dioxide (CO₂), raw data. In: In supplement to: Köhler, P et al. (2017): A
618 156 kyr smoothed history of the atmospheric greenhouse gases CO₂, CH₄, and N₂O and their radiative
619 forcing. *Earth System Science Data*, 9(1), 363-387, <https://doi.org/10.5194/essd-9-363-2017>, PANGAEA,
620 2017.

621
622 Lam, P. and Bishop, J. K. B.: The continental margin is a key source of iron to the HNLC North Pacific Ocean,
623 Geophysical Research Letters, 35, 7, 2008.
624
625 Lambert, F., Delmonte, B., Petit, J.-R., Bigler, M., Kaufmann, P. R., Hutterli, M. A., Stocker, T. F., Ruth, U.,
626 Steffensen, J. P., and Maggi, V.: Dust-climate couplings over the past 800,000 years from the EPICA Dome C
627 ice core, Nature, 452, 616, 2008.
628
629 Lambert, F., Tagliabue, A., Shaffer, G., Lamy, F., Winckler, G., Farias, L., Gallardo, L., and De Pol-Holz, R.:
630 Dust fluxes and iron fertilization in Holocene and Last Glacial Maximum climates, Geophysical Research
631 Letters, 42, 6014-6023, 2015.
632
633 Langmann, B., Zakšek, K., Hort, M., and Duggen, S.: Volcanic ash as fertiliser for the surface ocean,
634 Atmospheric Chemistry and Physics, 10, 3891-3899, 2010.
635
636 Löfverström, M., Caballero, R., Nilsson, J., and Kleman, J.: Evolution of the large-scale atmospheric
637 circulation in response to changing ice sheets over the last glacial cycle, Climate of the Past, 10, 1453-1471,
638 2014.
639
640 Lupker, M., Aciego, S. M., Bourdon, B., Schwander, J., and Stocker, T.: Isotopic tracing (Sr, Nd, U and Hf) of
641 continental and marine aerosols in an 18th century section of the Dye-3 ice core (Greenland), Earth and
642 Planetary Science Letters, 295, 277-286, 2010.
643
644 Lüthi, D., Le Floch, M., Bereiter, B., Blunier, T., Barnola, J.-M., Siegenthaler, U., Raynaud, D., Jouzel, J.,
645 Fischer, H., and Kawamura, K.: High-resolution carbon dioxide concentration record 650,000–800,000 years
646 before present, Nature, 453, 379-382, 2008.
647
648 Mahowald, N. M., Engelstaedter, S., Luo, C., Sealy, A., Artaxo, P., Benitez-Nelson, C., Bonnet, S., Chen, Y.,
649 Chuang, P. Y., Cohen, D. D., Dulac, F., Herut, B., Johansen, A. M., Kubilay, N., Losno, R., Maenhaut, W.,
650 Paytan, A., Prospero, J. M., Shank, L. M., and Siefert, R. L.: Atmospheric Iron Deposition: Global Distribution,
651 Variability, and Human Perturbations, Annual Review of Marine Science, 1, 245-278, 2008.
652
653 Mahowald, N. M., Yoshioka, M., Collins, W. D., Conley, A. J., Fillmore, D. W., and Coleman, D. B.: Climate
654 response and radiative forcing from mineral aerosols during the last glacial maximum, pre-industrial,
655 current and doubled-carbon dioxide climates, Geophysical Research Letters, 33, 2006.
656
657 Manabe, S. and Broccoli, A.: The influence of continental ice sheets on the climate of an ice age, Journal of
658 Geophysical Research: Atmospheres, 90, 2167-2190, 1985.
659
660 Martin, J. H., Gordon, R. M., and Fitzwater, S. E.: Iron in Antarctic waters, Nature, 345, 156-158, 1990.
661 Martínez-García, A., Rosell-Melé, A., Jaccard, S. L., Geibert, W., Sigman, D. M., and Haug, G. H.: Southern
662 Ocean dust–climate coupling over the past four million years, Nature, 476, 312, 2011.
663
664 Martínez-García, A., Sigman, D. M., Ren, H., Anderson, R. F., Straub, M., Hodell, D. A., Jaccard, S. L.,
665 Eglinton, T. I., and Haug, G. H.: Iron fertilization of the Subantarctic Ocean during the last ice age, Science,
666 343, 1347-1350, 2014.
667
668 Mayewski, P. A., Meeker, L. D., Whitlow, S., Twickler, M. S., Morrison, M. C., Bloomfield, P., Bond, G., Alley,
669 R. B., Gow, A. J., and Meese, D. A.: Changes in atmospheric circulation and ocean ice cover over the North
670 Atlantic during the last 41,000 years, Science, 263, 1747-1751, 1994.
671

672 McDonald, D., Pedersen, T., and Crusius, J.: Multiple late Quaternary episodes of exceptional diatom
673 production in the Gulf of Alaska, Deep Sea Research Part II: Topical Studies in Oceanography, 46, 2993-
674 3017, 1999.

675

676 McManus, J. F., Francois, R., Gherardi, J.-M., Keigwin, L. D., and Brown-Leger, S.: Collapse and rapid
677 resumption of Atlantic meridional circulation linked to deglacial climate changes, Nature, 428, 834-837,
678 2004.

679

680 Méheust, M., Stein, R., Fahl, K., and Gersonde, R.: Sea-ice variability in the subarctic North Pacific and
681 adjacent Bering Sea during the past 25 ka: new insights from IP 25 and U k' 37 proxy records, arktos, 4, 8,
682 2018.

683

684 Méheust, M., Stein, R., Fahl, K., Max, L., and Riethdorf, J.-R.: High-resolution IP 25-based reconstruction of
685 sea-ice variability in the western North Pacific and Bering Sea during the past 18,000 years, Geo-Marine
686 Letters, 36, 101-111, 2016.

687

688 Miller, R. and Tegen, I.: Climate response to soil dust aerosols, Journal of climate, 11, 3247-3267, 1998.

689 Müller, J., Wagner, A., Fahl, K., Stein, R., Prange, M., and Lohmann, G.: Towards quantitative sea ice
690 reconstructions in the northern North Atlantic: A combined biomarker and numerical modelling approach,
691 Earth and Planetary Science Letters, 306, 137-148, 2011.

692

693 North Greenland Ice Core Project, M.: 50 year means of oxygen isotope data from ice core NGRIP. In:
694 Supplement to: North Greenland Ice Core Project Members (2004): High-resolution record of Northern
695 Hemisphere climate extending into the last interglacial period. Nature, 431, 147-151,
696 <https://doi.org/10.1038/nature02805>, PANGAEA, 2007.

697

698 Olgun, N., Duggen, S., Croot, P. L., Delmelle, P., Dietze, H., Schacht, U., Oskarsson, N., Siebe, C., Auer, A.,
699 and Garbe-Schönberg, D.: Surface ocean iron fertilization: the role of subduction zone and hotspot volcanic
700 ash and fluxes into the Pacific Ocean, Global Biogeochemical Cycles, 25, GB4001, 2011.

701

702 Rasmussen, S. O., Abbott, P. M., Blunier, T., Bourne, A. J., Brook, E., Buchardt, S. L., Buizert, C., Chappellaz,
703 J., Clausen, H. B., Cook, E., Dahl-Jensen, D., Davies, S. M., Guillevic, M., Kipfstuhl, S., Laepple, T., Seierstad, I.
704 K., Severinghaus, J. P., Steffensen, J. P., Stowasser, C., Svensson, A., Vallelonga, P., Vinther, B. M., Wilhelms,
705 F., and Winstrup, M.: A first chronology for the North Greenland Eemian Ice Drilling (NEEM) ice core, Clim.
706 Past, 9, 2713-2730, 2013.

707

708 Ren, H., Studer, A. S., Serno, S., Sigman, D. M., Winckler, G., Anderson, R. F., Oleynik, S., Gersonde, R., and
709 Haug, G. H.: Glacial-to-interglacial changes in nitrate supply and consumption in the subarctic North Pacific
710 from microfossil-bound N isotopes at two trophic levels, Paleoceanography, 30, 1217-1232, 2015.

711

712 Röthlisberger, R.: Ice core evidence for the extent of past atmospheric CO₂ change due to iron fertilisation,
713 Geophysical Research Letters, 31, 16, 2004.

714

715 Ruth, U.: Dust concentration in the NGRIP ice core. In: Supplement to: Ruth, Urs; Bigler, Matthias;
716 Röthlisberger, Regine; Siggaard-Andersen, Marie-Louise; Kipfstuhl, Sepp; Goto-Azuma, Kumiko; Hansson,
717 Margareta E; Johnsen, Sigfus J; Lu, Huayu; Steffensen, Jørgen Peder (2007): Ice core evidence for a very
718 tight link between North Atlantic and east Asian glacial climate. Geophysical Research Letters, 34, L03706,
719 <https://doi.org/10.1029/2006GL027876>, PANGAEA, 2007.

720

721 Ruth, U., Bigler, M., Röthlisberger, R., Siggaard-Andersen, M. L., Kipfstuhl, S., Goto-Azuma, K., Hansson, M.
722 E., Johnsen, S. J., Lu, H., and Steffensen, J. P.: Ice core evidence for a very tight link between North Atlantic
723 and east Asian glacial climate, Geophysical Research Letters, 34, 2007.

724

725 Sachs, J. P. and Anderson, R. F.: Increased productivity in the subantarctic ocean during Heinrich events,
726 Nature, 434, 1118-1121, 2005.
727

728 Schepanski, K.: Transport of mineral dust and its impact on climate, Geosciences, 8, 151, 2018.
729

730 Schüpbach, S., Fischer, H., Bigler, M., Erhardt, T., Gfeller, G., Leuenberger, D., Mini, O., Mulvaney, R.,
731 Abram, N. J., and Fleet, L.: Greenland records of aerosol source and atmospheric lifetime changes from the
732 Eemian to the Holocene, Nature communications, 9, 1476, 2018.
733

734 Serno, S., Winckler, G., Anderson, R. F., Hayes, C. T., McGee, D., Machalett, B., Ren, H., Straub, S. M.,
735 Gersonde, R., and Haug, G. H.: Eolian dust input to the Subarctic North Pacific, Earth and Planetary Science
736 Letters, 387, 252-263, 2014.
737

738 Serno, S., Winckler, G., Anderson, R. F., Maier, E., Ren, H., Gersonde, R., and Haug, G. H.: Comparing dust
739 flux records from the Subarctic North Pacific and Greenland: Implications for atmospheric transport to
740 Greenland and for the application of dust as a chronostratigraphic tool, Paleoceanography, 30, 583-600,
741 2015.
742

743 Shoenfelt, E. M., Sun, J., Winckler, G., Kaplan, M. R., Borunda, A. L., Farrell, K. R., Moreno, P. I., Gaiero, D.
744 M., Recasens, C., and Sambrotto, R. N.: High particulate iron (II) content in glacially sourced dusts enhances
745 productivity of a model diatom, Science advances, 3, e1700314, 2017.
746

747 Shoenfelt, E. M., Winckler, G., Lamy, F., Anderson, R. F., and Bostick, B. C.: Highly bioavailable dust-borne
748 iron delivered to the Southern Ocean during glacial periods, Proceedings of the National Academy of
749 Sciences, 115, 11180-11185, 2018.
750

751 Smetacek, V., Klaas, C., Strass, V. H., Assmy, P., Montresor, M., Cisewski, B., Savoye, N., Webb, A., d'Ovidio,
752 F., and Arrieta, J. M.: Deep carbon export from a Southern Ocean iron-fertilized diatom bloom, Nature, 487,
753 313-319, 2012.
754

755 Spolaor, A., Vallelonga, P., Cozzi, G., Gabrieli, J., Varin, C., Kehrwald, N., Zennaro, P., Boutron, C., and
756 Barbante, C.: Iron speciation in aerosol dust influences iron bioavailability over glacial-interglacial
757 timescales, Geophysical Research Letters, 40, 1618-1623, 2013.
758

759 Sun, W., Shen, J., Yu, S.-Y., Long, H., Zhang, E., Liu, E., and Chen, R.: A lacustrine record of East Asian
760 summer monsoon and atmospheric dust loading since the last interglaciation from Lake Xingkai, northeast
761 China, Quaternary Research, 89, 270-280, 2018.
762

763 Svensson, A., Biscaye, P. E., and Grousset, F. E.: Characterization of late glacial continental dust in the
764 Greenland Ice Core Project ice core, Journal of Geophysical Research: Atmospheres, 105, 4637-4656, 2000.
765 Talley, L. D.: Freshwater transport estimates and the global overturning circulation: Shallow, deep and
766 throughflow components, Progress in Oceanography, 78, 257-303, 2008.
767

768 Tsuda, A., Takeda, S., Saito, H., Nishioka, J., Nojiri, Y., Kudo, I., Kiyosawa, H., Shiimoto, A., Imai, K., and Ono,
769 T.: A mesoscale iron enrichment in the western subarctic Pacific induces a large centric diatom bloom,
770 Science, 300, 958-961, 2003.
771

772 Tulenko, J. P., Lofverstrom, M., and Briner, J. P.: Ice sheet influence on atmospheric circulation explains the
773 patterns of Pleistocene alpine glacier records in North America, Earth and Planetary Science Letters, 534,
774 116115, 2020.
775

776 Vallelonga, P., Barbante, C., Cozzi, G., Gabrieli, J., Schüpbach, S., Spolaor, A., and Turetta, C.: Iron fluxes to
777 Talos Dome, Antarctica, over the past 200 kyr, Clim. Past, 9, 597-604, 2013.

778
779 Vallelonga, P., Van de Velde, K., Candelone, J.-P., Morgan, V., Boutron, C., and Rosman, K.: The lead
780 pollution history of Law Dome, Antarctica, from isotopic measurements on ice cores: 1500 AD to 1989 AD,
781 Earth and Planetary Science Letters, 204, 291-306, 2002.
782
783 Watanabe, O., Jouzel, J., Johnsen, S., Parrenin, F., Shoji, H., and Yoshida, N.: Homogeneous climate
784 variability across East Antarctica over the past three glacial cycles, Nature, 422, 509-512, 2003.
785
786 Wolff, E. W., Fischer, H., Fundel, F., Ruth, U., Twarloh, B., Littot, G. C., Mulvaney, R., Röthlisberger, R., De
787 Angelis, M., and Boutron, C. F.: Southern Ocean sea-ice extent, productivity and iron flux over the past
788 eight glacial cycles, Nature, 440, 491-496, 2006.
789
790 Xiao, C., Du, Z., Handley, M. J., Mayewski, P. A., Cao, J., Schüpbach, S., Zhang, T., Petit, J. -R., Li, C., and Han,
791 Y.: Iron in the NEEM ice core relative to Asian loess records over the last glacial -interglacial cycle, National
792 Science Review, 2020. 2020.
793
794 Xiao, J., An, Z., Liu, T., Inouchi, Y., Kumai, H., Yoshikawa, S., and Kondo, Y.: East Asian monsoon variation
795 during the last 130,000 years: evidence from the Loess Plateau of central China and Lake Biwa of Japan,
796 Quaternary Science Reviews, 18, 147-157, 1999.
797
798 Yoon, J.-E., Yoo, K.-C., Macdonald, A. M., Yoon, H.-I., Park, K.-T., Yang, E. J., Kim, H.-C., Lee, J. I., Lee, M. K.,
799 and Jung, J.: Reviews and syntheses: Ocean iron fertilization experiments—past, present, and future looking
800 to a future Korean Iron Fertilization Experiment in the Southern Ocean (KIFES) project, Biogeosciences, 15,
801 5847-5889, 2018.
802
803 Young, R., Carder, K., Betzer, P., Costello, D., Duce, R., DiTullio, G., Tindale, N., Laws, E., Uematsu, M., and
804 Merrill, J.: Atmospheric iron inputs and primary productivity: Phytoplankton responses in the North Pacific,
805 Global Biogeochemical Cycles, 5, 119-134, 1991.
806
807 Yung, Y. L., Lee, T., Wang, C.-H., and Shieh, Y.-T.: Dust: A diagnostic of the hydrologic cycle during the Last
808 Glacial Maximum, Science, 271, 962-963, 1996.
809
810 Zahn, R., Pedersen, T. F., Bornhold, B. D., and Mix, A. C.: Water mass conversion in the glacial subarctic
811 Pacific (54° N, 148° W): Physical constraints and the benthic-planktonic stable isotope record,
812 Paleoceanography, 6, 543-560, 1991.
813
814 Zhang, X.-Y., Gong, S., Zhao, T., Arimoto, R., Wang, Y., and Zhou, Z.: Sources of Asian dust and role of
815 climate change versus desertification in Asian dust emission, Geophysical Research Letters, 30, 2003.
816
817 Zhang, X., Han, Y., Sun, Y., Cao, J., and An, Z.: Asian dust, eolian iron and black carbon — Connections to
818 climate changes. In: Late Cenozoic Climate Change in Asia, Springer, 2014.

819

820

821